Two-dimensional topological insulator state in double HgTe quantum well

G. M. Gusev [1], E. B. Olshanetsky,[2] F. G. G. Hernandez [1], O. E. Raichev [3], N. N. Mikhailov,[2] and S. A. Dvoretsky [2]

[1]*Instituto de Física da Universidade de São Paulo, 135960-170 São Paulo, São Paulo, Brazil*
[2]*Institute of Semiconductor Physics, Novosibirsk 630090, Russia*
[3]*Institute of Semiconductor Physics, NAS of Ukraine, Prospekt Nauki 41, 03028 Kyiv, Ukraine*

The two-dimensional topological insulator phase has been observed previously in single HgTe-based quantum wells with inverted subband ordering. In double quantum wells (DQWs), coupling between the layers introduces additional degrees of freedom leading to a rich phase picture. By studying local and nonlocal resistance in HgTe-based DQWs, we observe both the gapless semimetal phase and the topological insulator phase, depending on parameters of the samples and according to theoretical predictions. Our work establishes the DQWs as a promising platform for realization of multilayer topological insulators.

Topological insulators (TIs) are a new class of materials characterized by an insulating band gap in the bulk, like in ordinary band insulators, but having topologically protected conducting states at their edges for two-dimensional (2D) TIs or at the surface for three-dimensional TIs [1–4]. The TI phase has been theoretically predicted [2] and experimentally realized in HgTe quantum wells (QWs) with $Cd_xHg_{1-x}Te$ barriers [5]. The crucial properties enabling the 2D TI states in these systems are the strong spin-orbit coupling that leads to inverted band structure of HgTe and the size quantization that opens the gaps in the electron spectrum of initially gapless HgTe. In HgTe-based QWs with the well width d above the critical one, $d > d_c$, the upper size-quantization subband of heavy holes stays above the electronlike subbands. This inverted subband ordering produces the 2D TI phase with one-dimensional edge states inside the gap in the bulk 2D subband spectrum. Electron transport in the edge states is expected to be highly ballistic because the elastic backscattering of electrons is forbidden due to the time reversal symmetry in the absence of magnetic field and magnetic impurities. Experimental manifestations of the edge transport are the quantization of conductance at the universal value $2e^2/h$ and the appearance of nonlocal voltage away from the dissipative bulk current path [5,6].

Double quantum wells (DQWs) are bilayer systems consisting of two QWs separated by a tunneling-transparent barrier. Theoretical studies suggest [7] that the picture of phase states in these structures is strongly affected compared to the single QW case and becomes more rich because of the additional degrees of freedom associated with an increase in the number of 2D subbands and tunnel-induced hybridization between them. In particular, the subband ordering depends not only on the well width d and Cd content in the barriers x_{Cd} but also on the barrier thickness t, and is sensitive to the asymmetry induced, for example, by a transverse electric field. Figures 1(a) and 1(b) show a typical dependence of subband edges on t at a fixed d for symmetric HgTe-based wells (see [8] for the details of calculations). The electronlike

subbands E1 and E2, formed as a result of coupling between the Γ_6 states and the light hole part of Γ_8 states, are characterized by the wave functions which strongly penetrate into the barriers and, therefore, show a significant tunnel-induced splitting. In contrast, the hole subbands H1–H4, originating from the heavy hole part of Γ_8 states, are characterized by the wave functions weakly penetrating into the barriers because of the large effective mass. Thus, the tunnel-induced splitting of the pairs of subbands H1–H2 and H3–H4 exists only at very small t, while for $t > 2$ nm their energies are the same as in the single QWs. The degeneracy of H1 and H2 subbands is lifted at nonzero wave vector **k**, forming two branches with the opposite dispersion in the case of mixed ordering of subbands E1–H2–H1–E2, which results in a gapless energy spectrum, Fig. 1(c). With increasing t and/or d, a fully inverted ordering E1–E2–H2–H1 is realized, and a gapped TI phase appears, Fig. 1(d). The energy spectrum in the gapless phase resembles the bilayer graphene spectrum [9] with the absence of valley degeneracy [10].

Similar as in bilayer graphene [13], it is predicted that the gapless phase in symmetric HgTe DQWs can be transformed into a gapped phase by breaking the inversion symmetry of two wells via a transverse electric field due to asymmetric doping or external gate biasing [7,14]. Since the gap energy depends on the field, both these systems are the tunable gap semiconductors. However, there is a principal difference between the biased bilayer graphene and asymmetric HgTe DQWs: in the latter case the topologically protected edge states appear in the gap. Indeed, in contrast to bilayer graphene, HgTe-based DQWs possess topological properties due to subband inversion, and the calculations based on the effective Hamiltonian models [7,14,15] show coexistence of the bulk and edge states in the gapless semimetal phase. Thus, it is expected that opening the gap in HgTe DQWs by the field makes them 2D TIs, where the edge state transport can be detected experimentally.

In this Rapid Communication we present the results of studies of the local and nonlocal resistance in HgTe-based
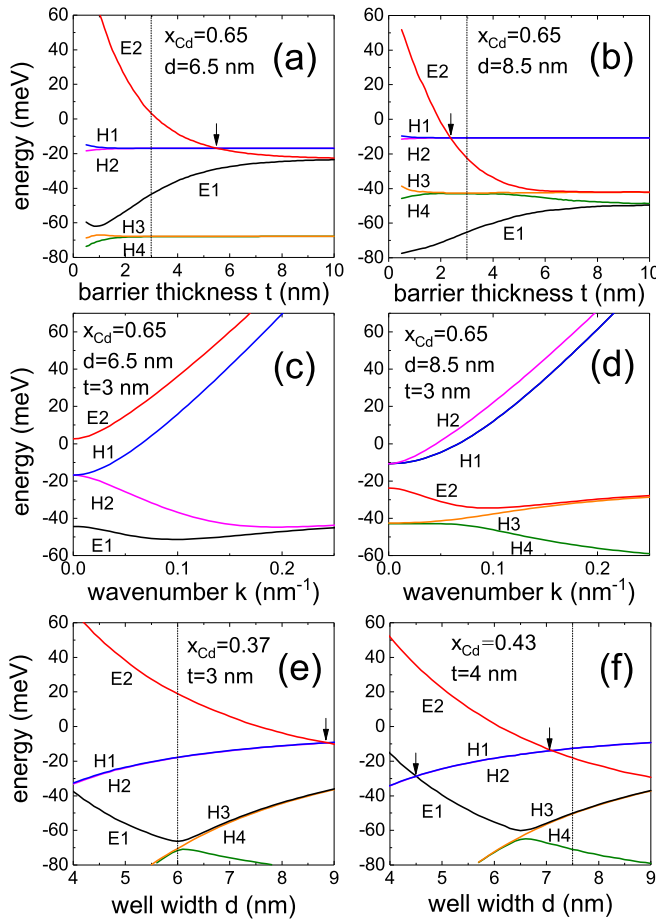
FIG. 1. Calculated band structure for symmetric [013]-grown HgTe/Cd$_x$Hg$_{1-x}$Te DQWs with different well widths d, barrier thicknesses t, and Cd content in the barriers. (a) and (b) Dependence of subband energies at $k = 0$ on t. (c) and (d) Subband dispersion for $\mathbf{k}||[100]$. (e) and (f) Dependence of subband energies at $k = 0$ on d. The arrows show the points of subband inversion leading to phase transitions, and the vertical lines correspond to parameters of the DQWs studied in our experiment.

DQWs. By studying several groups of samples with different parameters x_{Cd}, d, and t, we have observed both the gapped phase and the gapless semimetal phase, clearly distinguished by the temperature dependence of the local resistance. By measuring nonlocal resistance in the gapped samples, we confirm the edge state transport in the absence of magnetic field, thereby providing the experimental evidence of the 2D TI phase in HgTe DQWs. Furthermore, we observe the gap and the edge state transport in the DQWs which are expected to be in the gapless phase if the transverse electric field were absent.

Double quantum wells HgTe/Cd$_x$Hg$_{1-x}$Te with [013] surface orientation and equal well widths from 6.0 to 8.5 nm were prepared by molecular beam epitaxy (MBE) [8]. The layer thicknesses were determined by ellipsometry during the MBE growth, with the accuracy ±0.3 nm. The devices are designed for multiterminal measurements and contain three 3.2 μm wide consecutive segments of different length (2, 8, and 32 μm) and nine contacts (Fig. 2) shunting both QW layers. A dielectric layer, 200 nm of SiO$_2$, was deposited on the
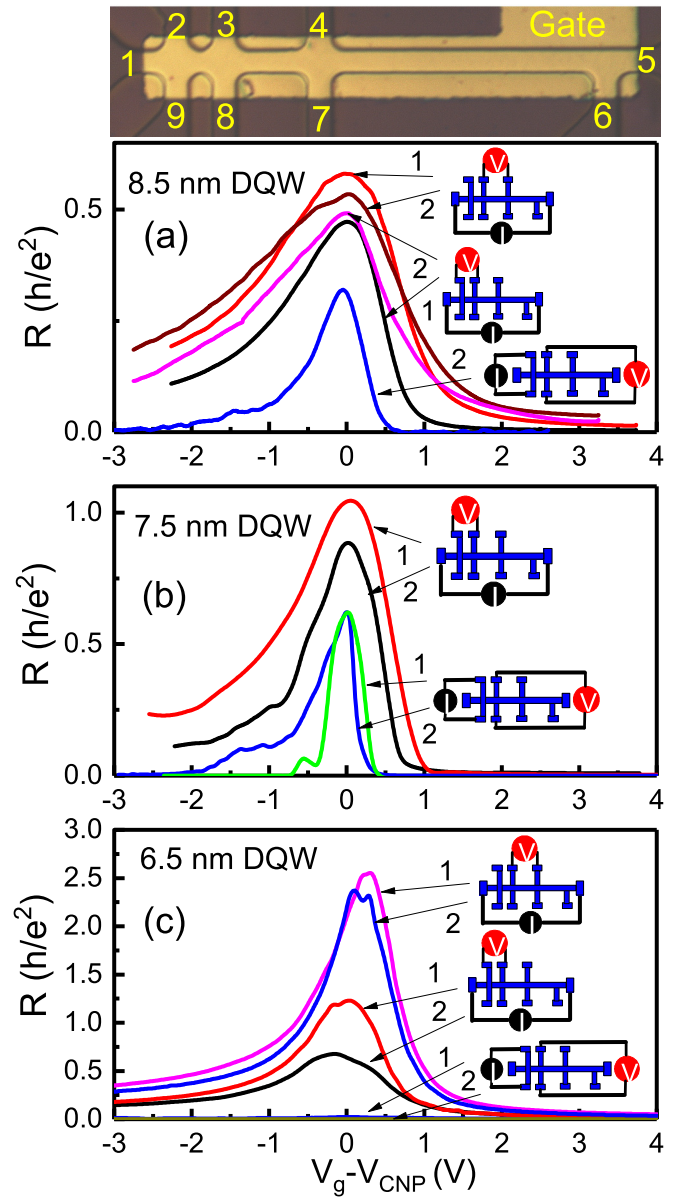

FIG. 2. Resistance at $T = 4.2$ K as a function of the gate voltage V_g for different configurations of measurements and for different devices (1,2) fabricated from DQW structures with $d = 8.5$ nm (a), $d = 7.5$ nm (b), and $d = 6.5$ nm (c). The top panel shows the device layout and numbering of the probes.

sample surface and then covered by a TiAu gate. The density variation with the gate voltage was 0.86×10^{11} cm^{-2} V^{-1}. The transport measurements were performed in the range of temperatures T from 1.4 to 70 K by using a standard four-point circuit with 1–13 Hz AC current of 1–10 nA through the sample, which is sufficiently low to avoid overheating effects. For each set of parameters, results for two typical devices (1,2) are represented. Table I lists parameters of the devices, including the gate voltage corresponding to the charge neutrality point (CNP) at $T = 4.2$ K.

Figure 2 presents the local and nonlocal resistances at zero magnetic field for the samples fabricated from the structures with $d = 8.5$ nm, $d = 7.5$ nm, and $d = 6.5$ nm. In the local

TABLE I. Parameters of HgTe/Cd$_x$Hg$_{1-x}$Te DQWs.

d (nm)	t (nm)	x_{Cd}	V_{CNP} (V)	Properties
8.5	3	0.65	-0.7	TI
7.5	4	0.43	-0.8	narrow-gap TI
6.5	3	0.65	-5	gapless
6.0	3	0.37	-2.4	TI

configuration, the current I flows between the contacts 1 and 5, and the voltage V is measured between the short distance separated probes 2 and 3, $R_L = R_{1,5}^{2,3} = V_{2,3}/I_{1,5}$, and between widely separated probes 3 and 4, $R_L = R_{1,5}^{3,4} = V_{3,4}/I_{1,5}$. In the nonlocal configuration, the current flows between the contacts 2 and 9 while the voltage is measured between the probes 3 and 8, $R_{NL} = R_{2,9}^{3,8} = V_{3,8}/I_{2,9}$. A slower decrease of the resistances with V_g in the negative voltage region is related to a larger density of states in the valence band.

We first focus on the results obtained in DQWs with $d = 8.5$ and 7.5 nm. In the first one, the peaks of the resistances $R_{1,5}^{2,3}$ and $R_{1,5}^{3,4}$ are close to the quantity $5/9(h/e^2)$ expected in the case of purely ballistic edge state transport in the multiprobe device shown in Fig. 2, though $R_{1,5}^{3,4}$ is larger than $R_{1,5}^{2,3}$. In the second one, the peak resistance $R_{1,5}^{2,3}$ is considerably larger than $5/9(h/e^2)$. These observations contradict with the picture of ballistic edge state transport in 2D TIs implying that the backscattering is forbidden at sufficiently low temperatures [1–4] so the resistance is independent of the distance between the voltage probes. While some experimental works indeed confirm the quantized transport in multiprobe HgTe QW devices [6,16], the longest edge channel length that shows a quantized resistance peak never exceeds 10 μm. We notice that the edge current in our experiment flows along the gated sample edge (see the top of Fig. 2), so the effective length L_{nm} of the edge channel segments between the probes n and m is longer than the geometrical distance (bulk current path) between these probes and is estimated as $L_{23} \simeq 6$ μm and $L_{34} \simeq 12$ μm [8]. Thus, the absence of ballisticity is expectable.

The lack of robustness of the ballistic edge state transport has attracted a lot of attention, and numerous explanations have been proposed in recent years [17]. A detailed discussion of the existing theoretical models is beyond the scope of our paper. We emphasize that the edge state transport persists in both ballistic and diffusive regimes, while the values of local and nonlocal resistances depend on the sample design and measurement configurations. The most important characteristic feature of the 2D TIs, indicating the presence of the edge state transport, is the existence of nonlocal resistance of the order of resistance quantum h/e^2 [6]. We observe such nonlocal resistances in 8.5 and 7.5 nm DQWs. Figures 2(a) and 2(b) shows a significant difference between R_L and R_{NL}: the peaks of R_{NL} are narrower and this resistance disappears outside the bulk gap, where the edge channels are short circuited by the bulk conduction. Similar results were obtained for other nonlocal measurement configurations.

The Landauer-Büttiker formalism [18] allows one to find the resistance for any measurement configuration in multiprobe samples, by taking into account a finite probability of backscattering described by the mean free path length l [8]:

$$R_{n,m}^{i,j} \equiv \frac{V_{i,j}}{I_{n,m}} = \frac{h}{e^2} \frac{(N_{ij} + L_{ij}/l)(N_{nm} + L_{nm}/l)}{N + L/l}. \quad (1)$$

Here N_{ij} and L_{ij} (or N_{nm} and L_{nm}) are the number of edge channel segments and their total length between the voltage (or current) leads along the arc that does not contain the current (or voltage) leads. Next, N is the total number of segments, which is equal to the total number of leads, and L is the total length of all segments, i.e., the perimeter of the sample. In the ballistic transport limit, $L_{ij}/l \ll N_{ij}$, the resistance is an integer fraction of h/e^2 [6,16], while in the general case the resistance is sensitive to L_{ij} and is larger than the ballistic one. However, a comparison of Eq. (1) to the experimental peak resistances does not show a general agreement. The deviations are strong for the nonlocal configuration, where the ballistic limit corresponds to $R_{2,9}^{3,8} = 10/9(h/e^2)$ while the measured resistances are not larger than this value, as expected from Eq. (1) [8], but, in fact, are considerably smaller. This means that the backscattering within the edge channel alone cannot explain the transport, and the other processes responsible for attenuation of the voltage signal, such as edge to bulk leakage of electrons and bulk current contribution, are important. Nevertheless, the very existence of nonlocal resistance is a sufficient proof for the domination of the edge transport near CNP in the samples with $d = 8.5$ nm and $d = 7.5$ nm, which also suggests the presence of the bulk gaps.

Now we turn to the observations for DQW structure with $d = 6.5$ nm, Fig. 2(c), which differs from the structure of Fig. 2(a) only by the well width. One can see that the ratio $R_{1,5}^{3,4}/R_{1,5}^{2,3}$ is close to the ratio of the distances between the probes, which suggests the dominance of the bulk transport. More important, the nonlocal resistance is absent. This is the property associated with zero gap spectrum, shown in Fig. 1(c) for this structure. Unlike the edge state conductivity in 8.5 and 7.5 nm DQWs, the conductivity in 6.5 nm devices is due to the bulk, while the edge contribution is short circuited.

For a further proof of the different nature of the transport in the samples with open and closed bulk gap, we have measured the temperature dependence of the resistance near CNP. The variation of the resistance with the gate voltage and temperature is shown in Fig. 3. The evolution of the resistance in the samples with $d = 8.5$ nm and $d = 7.5$ nm resembles that for single well 2D TIs [16,19]. For 8.5 nm sample, the resistance decreases sharply at $T > 20$ K while saturating below 15 K. For 7.5 nm sample, a decrease in the resistance with T starts below 10 K, indicating a small mobility gap of 0.5–1 meV. Fitting the resistance dependence on T by the activation law $R \sim \exp(\Delta/2k_BT)$, we find the activation gap $\Delta = 15$ meV for 8.5 nm DQW and $\Delta = 0.5$ meV for 7.5 nm DQW. These values agree with calculated gap energies (see Fig. 1), taking into account the ±0.3 nm uncertainty in the knowledge of t and d. Below 10 K the conductance is saturated with temperature, demonstrating no significant temperature dependence, which also agrees with the resistance behavior in single well 2D TIs [8,19]. Therefore, the temperature dependence of the resistance in 8.5 and 7.5 nm DQWs justifies that the bulk gap exists so that the transport through the edge channels is expectable.
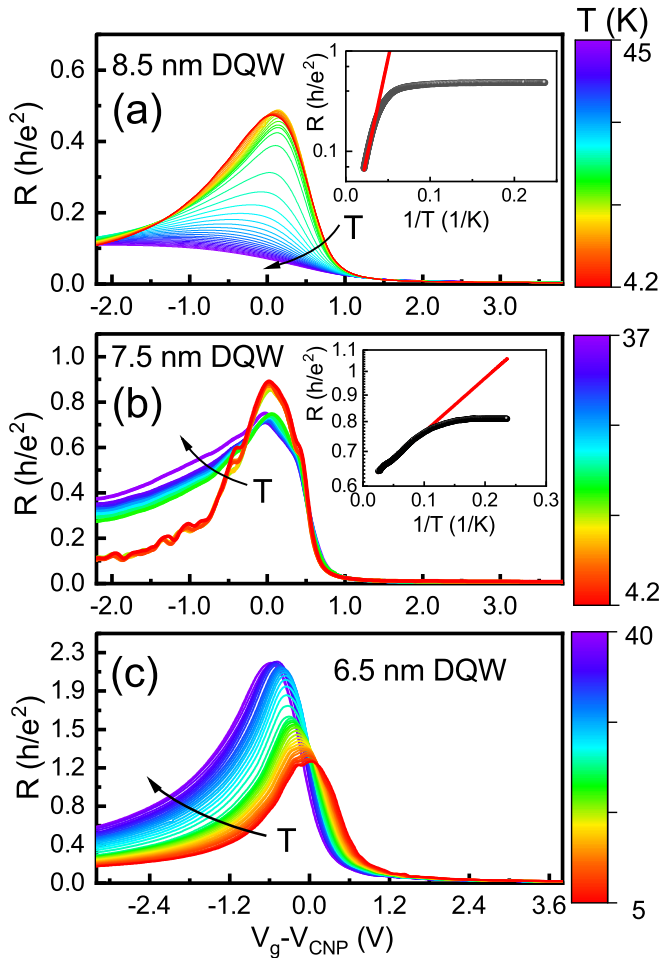
FIG. 3. Resistance as a function of the gate voltage for different temperatures for the DQWs with $d = 8.5$ nm, device 1 (a), $d = 7.5$ nm, device 2 (b), and $d = 6.5$ nm, device 1 (c). The insets show the resistance at CNP as a function of $1/T$, the red lines correspond to $R \sim \exp(\Delta/2k_B T)$ with $\Delta \simeq 15$ meV (a) and $\Delta \simeq 0.5$ meV (b).

The DQWs with $d = 6.5$ nm demonstrate the opposite temperature dependence: the resistance increases with increasing T, indicating a metallic type of conductivity. A similar behavior is seen [8] in a single HgTe well with critical width $d \simeq d_c$, which is a gapless Dirac fermion system. With increasing T, the resistance peak in Fig. 3(c) shifts to the hole side and becomes wider. This behavior is related to asymmetry of the energy spectrum, and described within the bulk transport picture as follows. The bulk resistance reaches a maximum when the chemical potential stays in the point where the bands touch each other. As the density of states in the valence band is larger, for this position of the chemical potential the hole density is larger than the electron one, and the difference in the densities increases with T. Thus, the gate voltage corresponding to the peak resistance is shifted away from the CNP to the hole side. In summary, the temperature dependence of the resistance in 6.5 nm DQWs justifies that the gap is closed and the transport occurs through the bulk.

Finally, we present the results for DQWs with $d = 6$ nm (Fig. 4), which show a special behavior. According to our
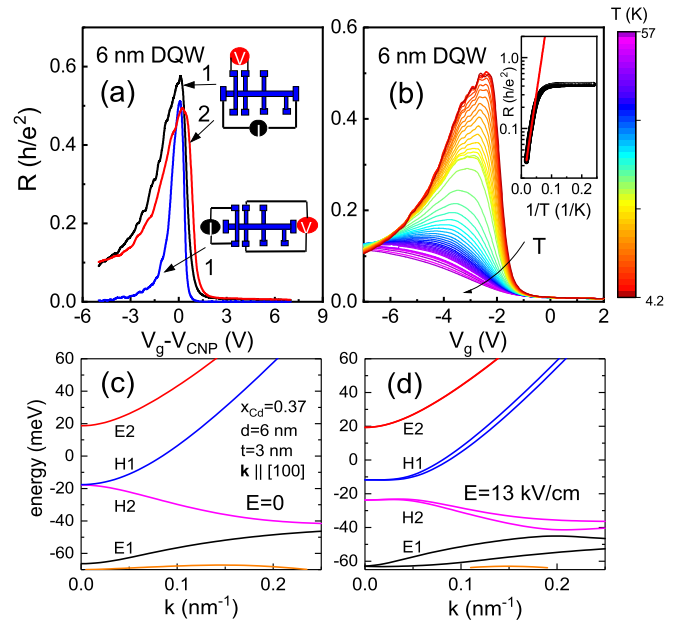

FIG. 4. Experimental data and energy spectrum calculations for DQW structure with $d = 6$ nm: local and nonlocal resistances as functions of the gate voltage at $T = 4.2$ K (a), the evolution of the local resistance of device 2 with temperature and the dependence of the resistance at CNP on $1/T$ (b), the energy spectrum for symmetric structure (c), and the energy spectrum in the presence of a transverse electric field $E = 13$ kV/cm (d).

calculations [Figs. 1(e) and 4(c)], this structure is expected to be a gapless semimetal, while the transport measurements demonstrate that it is actually a 2D TI with the activation gap $\Delta = 11$ meV and a nonlocal response similar to those in Figs. 2(a) and 2(b). This finding can be explained by the presence of an asymmetry, presumably related to specifics of MBE growth for this particular structure, for example, an uncontrollable chemical doping. Calculations of the energy spectrum of asymmetric DQWs confirm this assumption and show that the observed gap can be created by a transverse electric field $E = 13$ kV/cm, which splits the heavy hole subbands H1 and H2 apart and also leads to Rashba spin splitting of all the subbands, Fig. 4(d). This explanation is the most natural one, and we cannot propose any other explanation of the experimental facts. While in bilayer graphene the transverse electric field can be controlled by double gates [20], fabrication of the devices with controllable gap based on MBE-grown HgTe DQWs requires numerous technological efforts. A forthcoming development of double gating technology for HgTe DQWs can open a possibility for electrical control of the edge state transport, which is important both for fundamental physics and for device applications.

In conclusion, we have demonstrated phase diversity in HgTe DQWs by observing both a topological insulator phase and a gapless semimetal phase that resembles the bilayer graphene. We have also detected a topological insulator phase whose existence requires the presence of a transverse asymmetry of DQWs, possibly produced by an internal electric field. We believe that our studies

will be helpful for paving the way to the tunable topological insulators and the multilayer topological insulators.

[1] C. L. Kane and E. J. Mele, Phys. Rev. Lett. **95**, 146802 (2005); **95**, 226801 (2005).

[2] B. A. Bernevig and S. C. Zhang, Phys. Rev. Lett. **96**, 106802 (2006); B. A. Bernevig, T. L. Hughes, and S. C. Zhang, Science **314**, 1757 (2006).

[3] M. Z. Hasan and C. L. Kane, Rev. Mod. Phys. **82**, 3045 (2010); X.-L. Qi and S.-C. Zhang, *ibid.* **83**, 1057 (2011).

[4] X.-L. Qi and S.-C. Zhang, Phys. Today **63**(1), 33 (2010).

[5] M. Konig, S. Wiedmann, C. Brune, A. Roth, H. Buhmann, L. W. Molenkamp, X.-L. Qi, and S.-C. Zhang, Science **318**, 766 (2007).

[6] A. Roth, C. Brune, H. Buhmann, L. W. Molenkamp, J. Maciejko, X.-L. Qi, and S.-C. Zhang, Science **325**, 294 (2009).

[7] S. S. Krishtopenko, W. Knap, and F. Teppe, Nat. Sci. Rep. **6**, 30755 (2016).

[8] See Supplemental Material at http://link.aps.org/supplemental/10.1103/PhysRevB.101.241302 for description of the samples, details of the transport measurements, the results of measurements for single quantum wells and includes Refs. [21–25].

[9] A. H. Castro Neto, F. Guinea, N. M. R. Peres, K. S. Novoselov, and A. K. Geim, Rev. Mod. Phys. **81**, 109 (2009).

[10] A different kind of gapless semimetal can be created in a single HgTe QW by application of a strong in-plane magnetic field [11,12], in this case the spin degeneracy is missed as well.

[11] O. E. Raichev, Phys. Rev. B **85**, 045310 (2012).

[12] G. M. Gusev, E. B. Olshanetsky, Z. D. Kvon, O. E. Raichev, N. N. Mikhailov, and S. A. Dvoretsky, Phys. Rev. B **88**, 195305 (2013).

[13] E. V. Castro, N. M. R. Peres, J. M. B. Lopes dos Santos, F. Guinea, and A. H. Castro Neto, J. Phys.: Conf. Ser. **129**, 012002 (2008).

[14] P. Michetti, J. C. Budich, E. G. Novik, and P. Recher, Phys. Rev. B **85**, 125309 (2012); P. Michetti and B. Trauzettel, Appl. Phys. Lett. **102**, 063503 (2013).

[15] Y. Baum, T. Posske, I. C. Fulga, B. Trauzettel, and A. Stern, Phys. Rev. Lett. **114**, 136801 (2015).

[16] E. B. Olshanetsky, Z. D. Kvon, G. M. Gusev, A. D. Levin, O. E. Raichev, N. N. Mikhailov, and S. A. Dvoretsky, Phys. Rev. Lett. **114**, 126802 (2015).

[17] J. Maciejko, C. Liu, Y. Oreg, X.-L. Qi, C. Wu, and S.-C. Zhang, Phys. Rev. Lett. **102**, 256803 (2009); Y. Tanaka, A. Furusaki, and K. A. Matveev, *ibid.* **106**, 236402 (2011); V. Cheianov and L. I. Glazman, *ibid.* **110**, 206803 (2013); A. Strom, H. Johannesson, and G. I. Japaridze, *ibid.* **104**, 256804 (2010); N. Lezmy, Y. Oreg, and M. Berkooz, Phys. Rev. B **85**, 235304 (2012); F. Crepin, J. C. Budich, F. Dolcini, P. Recher, and B. Trauzettel, *ibid.* **86**, 121106(R) (2012); J. I. Vayrynen, M. Goldstein, and L. I. Glazman, Phys. Rev. Lett. **110**, 216402 (2013); A. M. Lunde and G. Platero, Phys. Rev. B **88**, 115411 (2013); S. Essert, V. Krueckl, and K. Richter, *ibid.* **92**, 205306 (2015); P. P. Aseev and K. E. Nagaev, *ibid.* **94**, 045425 (2016); J. Wang, Y. Meir, and Y. Gefen, Phys. Rev. Lett. **118**, 046801 (2017); P. Novelli, F. Taddei, A. K. Geim, and M. Polini, *ibid.* **122**, 016601 (2019).

[18] M. Büttiker, Phys. Rev. B **38**, 9375 (1988).

[19] G. M. Gusev, E. B. Olshanetsky, Z. D. Kvon, N. N. Mikhailov, and S. A. Dvoretsky, Phys. Rev. B **87**, 081311(R) (2013).

[20] P. Maher, L. Wang, Y. Gao, C. Forsythe, T. Taniguchi, K. Watanabe, D. Abanin, Z. Papi, P. Cadden-Zimansky, J. Hone, P. Kim, and C. R. Dean, Science **345**, 61 (2014).

[21] Z. D. Kvon, E. B. Olshanetsky, D. A. Kozlov, N. N. Mikhailov, and S. A. Dvoretskii, JETP Lett. **87**, 502 (2008).

[22] B. Büttner, C. X. Liu, G. Tkachov, E. G. Novik, C. Brüne, H. Buhmann, E. M. Hankiewicz, P. Recher, B. Trauzettel, S. C. Zhang, and L. W. Molenkamp, Nat. Phys. **7**, 418 (2011).

[23] D. A. Kozlov, Z. D. Kvon, N. N. Mikhailov, and S. A. Dvoretskii, JETP Lett. **96**, 730 (2012).

[24] E. G. Novik, A. Pfeuffer-Jeschke, T. Jungwirth, V. Latussek, C. R. Becker, G. Landwehr, H. Buhmann, and L. W. Molenkamp, Phys. Rev. B **72**, 035321 (2005).

[25] C. Brüne, C. X. Liu, E. G. Novik, E. M. Hankiewicz, H. Buhmann, Y. L. Chen, X. L. Qi, Z. X. Shen, S. C. Zhang, and L. W. Molenkamp, Phys. Rev. Lett. **106**, 126803 (2011).